Visualization of bat “echo space” using acoustic simulation

Yu Teshima (yuteshima18@gmail.com)
Doshisha University https://orcid.org/0000-0002-1202-470X
Yasufumi Yamada
Hiroshima University
Takao Tsuchiya
Doshisha University
Olga Heim
Doshisha University
Shizuko Hiryu
Doshisha University

Article

Keywords: echolocation, bats, flight navigation

Posted Date: June 2nd, 2021

DOI: https://doi.org/10.21203/rs.3.rs-512467/v1

Visualization of bat “echo space” using acoustic simulation

Abstract

Behavioral experiments with acoustic measurements have revealed the intriguing strategies of flight navigation and the use of ultrasound by echolocating bats in various environments. However, the echolocation behavior of bats has not been thoroughly investigated in regard to the environment they perceive via echolocation because it is technically difficult to measure all the echoes that reach the bats during flight, even with the conventional telemetry microphones currently in use. Therefore, we attempted to reproduce the echoes of bats during flight by combining acoustic simulation and behavioral experiments with acoustic measurements. As a result, we visualized the spatiotemporal changes in the echo incidence points detected by bats during flight, which enabled us to investigate the “echo space” revealed through echolocation. In addition, we could observe how the distribution of visualized echoes concentrated at the obstacle edges after the bats became more familiar with their environment. Furthermore, our results indicate that the direction of preceding echoes affects the turn rates of the bat's flight path, revealing their original echolocation behavior.

Introduction

Humans rely heavily on vision as a result of their exceptionally high visual acuity [1]. This superiority of human vision has guided the direction of technological development

in recent years. For instance, image recognition and simultaneous localization and mapping technologies using stereo and monocular cameras, such as automated driving, have advanced rapidly, particularly in combination with deep learning [2,3]. The accuracy of image processing technology has significantly improved in recent years and hence, is an important technological element in the field of sensing.

In contrast to humans, other animals optimize their behavior in weak vision or grasp their environment with sensory organs other than vision. For instance, echolocating bats mainly operate in the dark (e.g., caves and at night) where they cannot rely on vision but can perceive their environment via acoustic sensing using ultrasound [4]. Knowledge about a bat's sonar system has been accumulated through various experiments that, for instance, determined how bats alter ultrasound characteristics in response to various situations [5–7] and quantitatively measured the high acoustic acuity of the bat's sonar [8,9]. Using the basic principle of sensing with one transmitter and two receivers, bats can estimate object distance based on the echo delay time [10,11] and can localize objects by relying on the information difference between the echoes reaching the left and right ears [12]. This simple principle is also commonly used in the field of engineering, so that the bat's sonar has been proposed as a model for object localization [13] and obstacle avoidance algorithms [14,15], and is practically applied to an autonomous robot [16–18]. Ultrasonic sensing has been widely utilized to perceive our environment in a simple manner, as it is relatively inexpensive to produce and handles a much smaller amount of data compared to methods based on vision. Further improvements in acoustic sensing technology can be expected if knowledge of bat biosonar systems can be incorporated into the field of engineering.

Previous studies on the bats' behavior suggest that information about space or an object can differ depending on whether it was acquired via vision or echolocation. For instance, bats are known to collide with a smooth surface wall during flight [19] in cases where pulses are transmitted at a certain angle to the wall so that no echo is returned. In other words, a smooth surface wall is perceived as an empty space by bats, although the same wall can be perceived visually. In another example, nectar-feeding bats (*Glossophaga soricina*) were able to find the feeder in approximately half the time when the dish-shaped leaves of *Marcogravure ebenezer* were attached to the feeder. The dish-shaped leaves reflect echoes of similar intensity at wide angles and consequently make it easier for the bats to detect it [20]. These examples demonstrate how we can imagine the difference in perception based on sound and vision.

Since humans are highly focused on visual perception, one effective approach to better understand how the acoustic perception of bats works can be to visualize the world as perceived by sound. Thus it is necessary to focus on the echoes received by the bats rather than on the emitted pulses. Therefore, as one of the first studies, we aim at investigating the echolocation strategy of bats based on the information received from echoes. Since, it is difficult to measure all the echoes reaching both ears of a bat during flight, even with a conventional telemetry microphone [21] or an onboard acoustic logger [22], we propose a new approach. In particular, we propose to combine information from behavioral experiments (e.g. flight paths, emitted pulse directions) with acoustic simulation to estimate the echoes that reach the right and left ears of a bat in flight. Based on this acoustic simulation, we can reconstruct the locations and directions of echoes and

thus visualize the "echo space" as the entirety of these echoes. In addition, we examine how the echo space changes as the bats become more familiar with their environment.

Results

Bats (*Rhinolophus ferrumequinum nippon*) were allowed to fly repeatedly through a course with acrylic plates as obstacles, and their flight trajectories and pulse information (direction, intensity, and timing of emission) were measured [23]. The same obstacle course layout as in the behavioral experiment was constructed as a two-dimensional acoustic simulation space, and acoustic simulation was performed using the finite-difference time-domain (FDTD) method. With the information on the positions and pulses of the bats acquired in the behavioral experiment, we could determine the echoes that reached the positions of the right and left ears of the bats in flight in the simulation. Based on the left and right echo delay times we then estimated the echo incidence points and visualized them as the echo space (Supplementary Movie S1).

Spatial learning affects echo incidence point distribution

The echo incidence points were mostly concentrated near the inner edge of the obstacle wall (Fig. 1 & 2A,). Therefore, we selected those echo incidence points that were located within the inner half of the obstacle wall to investigate the effect of spatial learning on their distribution. We modeled the distance from the echo incidence points to the inner edge of the walls using generalized linear mixed effect models. We found that echo incidence points after spatial learning were located closer to the inner edge than before spatial learning ($contrast_{First/Last}$: ratio=1.2 ±0.07 SE, df=1053, t-ratio=3.6,

p<0.001, Fig. 2B). And the average distance of echo incidence points to the inner wall edge during the first flight was at 6.3 ± 0.4 SE cm, while it was at an average distance of 5.2 ± 0.3 SE cm during the last flight.

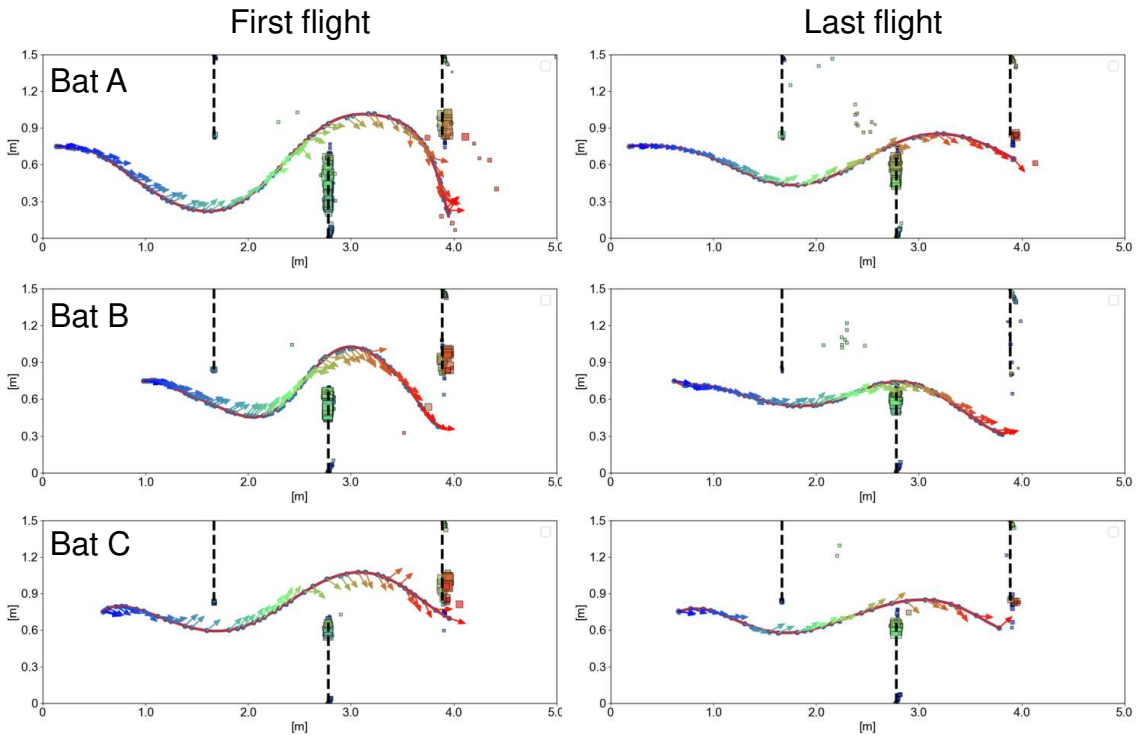

Figure 1. Flight direction, pulse directions, and echo incidence points during the first and last flight. Subplots of exemplary flight paths depict the flight directions (red solid lines), pulse directions (arrows), and echo incidence points (square plots) of individual bats (Bat A, Bat B, and Bat C) during the first flight and last flight. The color of the echo incidence points is the same as the color of the pulse from which the echo incidence point was generated, and its size is proportional to the sound pressure of the echo. Please note that one emitted pulse can result in several echo incidence points.

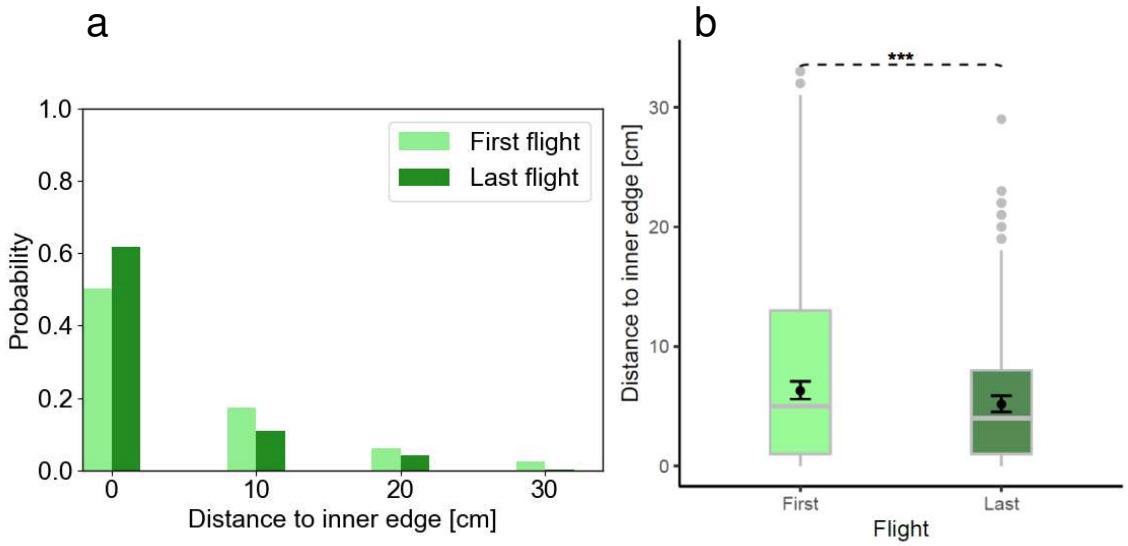

Figure 2. Distribution of echo incidence points on obstacle walls during the first and last flight. a The histogram shows the probability of echo incidence points being located at various distances to the inner edge of the obstacle (acrylic walls) during the first and last flight. **b** Box plots summarize data on the distances between echo incidence points and the inner edge within the inner half of obstacle walls for the first and last flight, while the black whisher plots represent model-related means (black circle) and associated 95% confidence intervals. These results are based on a model that fit the data well (based on residual plots) and that explained significantly more variance than its null model (χ^2=12.95, df=1, p<0.001). Also, the effect of the spatial-learning-factor in the model was found to be significant ($\chi^2_{\text{type-II-Wald}}$=13.0, df=1, p<0.001).

Flight path planning and spatial learning

It has been suggested in a previous study that the direction of pulse emission precedes the turn rate change in a bat's flight toward a target [24]. To investigate the relationship between the pulse and echo direction, respectively, and the turn rate, we also

117 plotted individual-specific time-series (Fig. 3A, B, see Supplementary Figs. S2, S3 for
118 data on all the individuals) and found that although both, pulse and echo direction change
119 precedes the turn rate change, the echo direction changes more smoothly and precedes the
120 turn rate change with a larger time lag than the pulse direction (Fig. 4A). To test this
121 observation statistically and to test for any effects of spatial learning, we determined the
122 individual-specific time delay τ_{max} at which a pulse or an echo direction, respectively, are
123 maximally correlated to a turn rate. After modeling τ_{max} as a function of the bat's
124 experience in interaction with the type of direction (echo or pulse), we found that, during
125 the first flight, pulse and echo direction changes preceded the turn rate change at 186 ±
126 54 ms and 377 ± 54 ms, respectively. In this case, the echo direction change tended to
127 precede the turn rate with a larger time lag than that of the pulse direction change
128 ($contrast_{Echo/Pulse}$: ratio=191 ± 68 SE, df=18, t-ratio=2.8, p=0.069, Fig. 4B). During the
129 last flight, the time lags between the pulse and echo direction change and the turn rate
130 change decreased slightly to 74 ± 54 ms and 233 ± 54 ms, respectively (Fig. 4B). Also,
131 the difference between time lags of echo and pulse direction changes decreased slightly
132 ($contrast_{Echo/Pulse}$: ratio=159 ± 68 SE, df=18, t-ratio=2.3, p=0.19, Fig. 4B). Based on the
133 inter-peak time lag difference between echo and pulse direction of 191 ms (= 377 ms –
134 186 ms) during the first flight, we estimate that an echo direction might affect the
135 direction of the fifth (4.6 ± 1.9) pulse following that echo. In contrast, we estimate that
136 the echo direction possibly affects the direction of the third (3.0 ± 1.6) pulse during the
137 last flight.

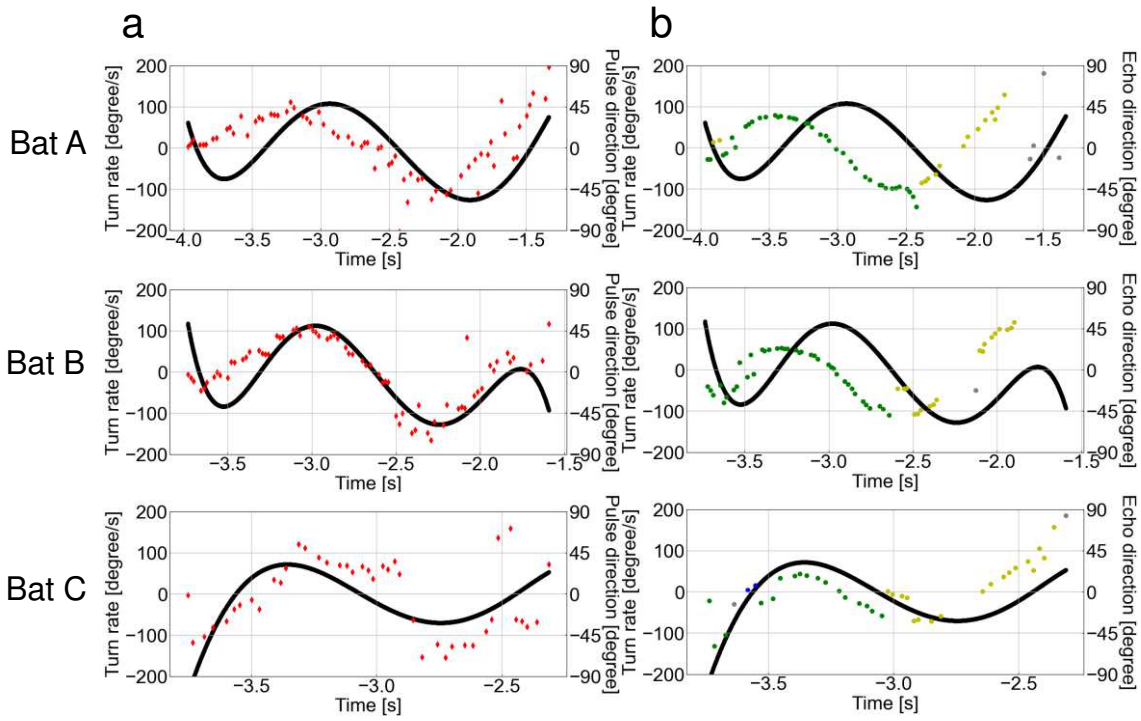

Figure 3. Time series plots of the pulse direction and turn rate, and echo direction and turn rate in the first flight. a Time series plot of the pulse direction (red rhombus plot) and turn rate (black solid line) in the first flight for each bat. **b** Time series plot of the echo direction (plotted) and turn rate (solid black line) for each bat in the first flight. The echo direction plot shows the echo incidence points with the highest sound pressure generated by a single pulse. The color of the echo direction plot depends on the obstacle (acrylic plate) on which the echo incidence is localized: blue indicates the first acrylic plate, green the second acrylic plate, yellow the third acrylic plate, and gray the echo source that was not localized on the obstacle.

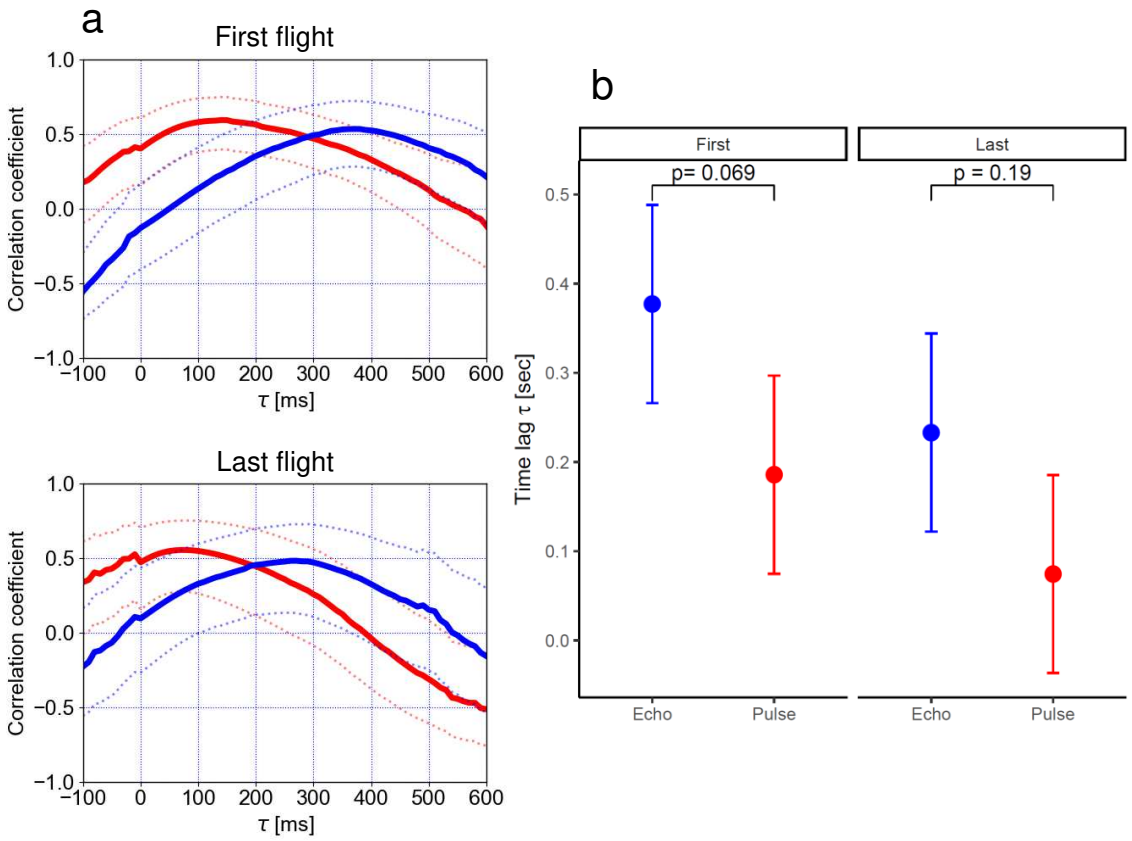

Figure 4. Correlation coefficients between the pulse direction and turn rate and between the echo direction and turn rate for the first and last flight. a Correlation coefficients between the pulse direction and turn rate (solid red line) and between the echo direction and turn rate (solid blue line). The dotted lines represent 95% confidence intervals. **b** The statistical comparison of individual-specific time lag data shows means (circles) and 95% confidence intervals (whiskers) for echo and pulse directions during the first and last flight. These results are based on a model that fit the data well (based on residual plots) and that explained significantly more variance than its null model (parametric bootstrap test, stat=16.0, df=3, p=0.007). The effect of the spatial-learning-factor in interaction with the type of information (echo or pulse) was found to be not significant ($\chi^2_{\text{type-II-Wald}}$=0.12, df=1, p=0.7) while the single effects showed a clear effect

(flight (first vs. last): $\chi^2_{\text{type-II-Wald}}=7.07$, df=1, p=0.008; information (echo vs. pulse): $\chi^2_{\text{type-II-Wald}}=13.25$, df=1, p<0.001).

Discussion

The aim of this paper is to use a new approach based on a combination of behavioral experiments and acoustic simulation in order to visualize the echo space and ultimately to gain more knowledge about how bats might perceive their environment acoustically. The results that we obtained using this new approach point towards differences between the information of surroundings acquired acoustically and visually. For instance, based on the echo incidence point distribution we found that bats appear to focus on the inner edges of the target walls when passing them, rather than scanning the entire obstacle which is usually happening when information is collected visually. Also, they seemed to focus more on the edge after spatial learning. We believe that a large number of pulses before spatial learning [23] resulted in a wider distribution of echo incidence points compared to the distribution after spatial learning where fewer pulses were emitted. Furthermore, we observed that depending on the characteristics of emitted pulses, such as the directivity or direction, the position and number of echo incidence points and consequently the contained information varies (Supplementary Movie S1). Also, the echo incidence point and the returning echo come not always from the same direction as the emitted pulse. This is different from the visually collected information, where the gaze direction is the same as the direction of reflected light [25]. Thus, together with previous studies that presented how echolocating bats misperceive objects [26], our

183 data demonstrate how different information from visually perceived objects can be to
184 information perceived via sound. Consequently, for understanding the behavior of a bat
185 flying through an obstacle course, not only the direction of emitted pulses but also the
186 location of generated echo incidence points should be considered at the same time.

187 In a previous study, it was shown that the number of pulses emitted during flight
188 decreased with progressing spatial learning [23], which appears to be in agreement with our
189 finding that the echo space also changed between the first and last flight. After bats have
190 become familiar with the obstacle course, the echo incidence points are concentrated at
191 the edge of the target, which is important for grasping the obstacle space. As a result, bats
192 seem to reduce the number of pulses necessary for collecting this information. Bats are
193 known to have spatial and shape memory [27–30]; therefore, by matching received
194 information with the memorized space, it could be possible to obtain the necessary
195 information about the space using a small number of pulses.

196 The bats are affected by not only the pulse direction but also the echo direction, and
197 the time of influence is earlier in the echo direction than in the pulse direction. This is a
198 natural result, considering that bats change the characteristics of the following pulse
199 based on information of the previous echoes. For instance, previous studies have
200 suggested that the Doppler shift compensation behavior is based on the echoes of the
201 previous one to three pulses [31], and in the bat's target direction anticipation behavior, the
202 model best matches the measured data when the target velocity is estimated from the
203 echoes of the previous five pulses [32]. In the present study and during the first flight, we
204 found a positive correlation peak of the pulse direction that preceded the turn rate change
205 by 186 ms, which is similar to the time lag obtained in an obstacle environment in a

206 previous study [33]. In contrast, the echo direction change preceded the turn rate change by
207 377 ms (Fig. 4A) which suggests that the effect of the pulse direction on the turn rate may
208 be a secondary result of the echo direction affecting the turn rate. Based on our results we
209 estimated that the echo direction possibly affects the direction of approximately the fifth
210 pulse during the first flight, which is consistent with the results of the above-mentioned
211 study [31,32]. In comparison the first flight, we found that the echo direction possibly affects
212 the direction of earlier pulses during the last flight. Thus bats might be able to reduce the
213 time required to determine the turn rates and pulse directions after the arrival of echoes
214 when they have become familiar with their surroundings.

215 In this study, we found that bats tend to focus more on the inner edges of obstacles
216 after spatial learning. Therefore, it is important to identify the edges of objects for object
217 recognition and avoidance. In the case of object identification using images from
218 cameras, there are many algorithms that can be used for edge extraction, such as the
219 Scale-Invariant Feature Transform [34]. In contrast, in sound object recognition, diffracted
220 waves are reflected from the edges as echoes in addition to a direct wave (see
221 Supplementary Fig. S4 and Supplementary Movie S1). In other words, in sound-based
222 object recognition, solely information from the direct wave and diffracted wave from the
223 edge is contained in the echoes. In contrast to object recognition by images, sound-based
224 methods may be more efficient because only minimal information is required. In this
225 study, we simulated the echoes and visualized echo space based on an engineering
226 approach; however, it is necessary to reproduce the actual process in bats more precisely
227 in the future, so that we can obtain a clearer understanding of the space perceived by bats.
228 For instance, we should include the directivity of the ear position by introducing the

head-related transfer function (HRTF) of the bat, including its ears, in the acoustic simulation space and a moving source to reflect the effect of the Doppler shift during flight to obtain more detailed spatial information. In addition, a bat auditory processing algorithm should be introduced into the post-echo processing such as the spectrogram correlation and transformation (SCAT) model [35–37]. We believe that this approach of echo simulation is a useful first step towards elucidating the perception space by bats.

Methods

Study species

Seven adult Japanese greater horseshoe bats (*Rhinolophus ferrumequinum nippon*, three males and four females) were used for the behavioral experiment. The bats of this species emit pulses consisting of a short initial FM component (iFM), a constant frequency component (CF), and a terminal FM component (tFM). These pulses are accompanied by overtones. Among the overtones, the second overtone, which has a CF component of approximately 68–70 kHz, has the highest sound pressure [21].

Experimental setup and procedure

The experiment was conducted in a corridor [4.5 m (L) × 1.5 m (W)] bordered by chains within a flight chamber [9 m (L) × 4.5 m (W) × 2.5 m (H)]. Three acrylic panels [1 m (W) × 2 m (H)] were placed in the corridor next to the chain-walls, alternating on the left and right side, with each panel being spaced 1 m apart from each other (Supplementary Fig. S5). The seven bats were allowed to fly one after the other from the

starting position through the obstacle course to a net behind the starting position 12 times. At the time of their first flight, they were completely unfamiliar with the obstacle course. Also, the experimenter carried each bat to the starting position of the flight while covering the bat with his hands to prevent it from collecting information about its surroundings. After a bat has flown through the course once, the experimenter immediately captured the bat using a 50 cm × 50 cm insect net. Then the bat was allowed to drink water from a plastic pipette and was brought back to the starting point by the experimenter who was covering them with their hands while carrying. During the experiment, only infrared lights were used in the flight chamber. Two high-speed video cameras (MotionPro X3; IDT Japan, Inc., Tokyo, Japan; 125 frames per second) recorded the flight paths of the bats, and microphones arranged in an array around the flight chamber recorded the emitted pulses of the bats to calculate the direction of pulse emission. We also calculated the pulse emission timing of the bats by measuring the pulses they emitted using a telemetry microphone attached to the bat's head. The methods were performed in accordance with the Principles of Animal Care (publication no. 86-23, revised 1985) issued by the National Institute of Health in the USA and regulations and pre-approved by the Animal Experiment Committee of Doshisha University. Please refer to the publication of Yamada et al. [23] for further methodological details.

Finite-difference time-domain (FDTD) method

We used the two-dimensional FDTD method to simulate the echoes that return to the positions of the right and left ear of bats during their flight. The FDTD method is one of the numerical methods developed by Yee to solve Maxwell's equations, which are the

governing equations of electromagnetic waves [38]. It has been widely used in the field of acoustics since Madariaga adapted it for elastic waves [39]. The method uses the governing equations of motion and the continuity of sound pressure as given in equations [1] and [2].

$$\frac{\partial \boldsymbol{p}}{\partial \boldsymbol{t}} + \boldsymbol{\rho c_0}^2 \nabla \cdot \boldsymbol{u} = \boldsymbol{0} \qquad [\boldsymbol{1}]$$

$$\frac{\partial \boldsymbol{u}}{\partial \boldsymbol{t}} + \frac{\boldsymbol{1}}{\boldsymbol{\rho}} \nabla \boldsymbol{p} = \boldsymbol{0} \qquad [\boldsymbol{2}]$$

where $\boldsymbol{p}$ is the sound pressure, $\boldsymbol{u}$ is the particle velocity vector, $\boldsymbol{\rho}$ is the medium density, and $\boldsymbol{c_0}$ is the speed of sound. The following equations are obtained by discretizing the above governing equations on a staggered grid.

$$\boldsymbol{p}_{i,j}^{n+1} = \boldsymbol{p}_{i,j}^{n} - \frac{\boldsymbol{\rho c_0}^2 \Delta \boldsymbol{t}}{\Delta} \left(\boldsymbol{u}_{x_{i+\frac{1}{2},j}}^{n+\frac{1}{2}} - \boldsymbol{u}_{x_{i-\frac{1}{2},j}}^{n+\frac{1}{2}} + \boldsymbol{u}_{y_{i,j+\frac{1}{2}}}^{n+\frac{1}{2}} - \boldsymbol{u}_{y_{i,j-\frac{1}{2}}}^{n+\frac{1}{2}} \right) \qquad [\boldsymbol{3}]$$

$$\boldsymbol{u}_{x_{i+\frac{1}{2},j}}^{n+\frac{1}{2}} = \boldsymbol{u}_{x_{i+\frac{1}{2},j}}^{n-\frac{1}{2}} - \frac{\Delta \boldsymbol{t}}{\boldsymbol{\rho}\Delta} \left(\boldsymbol{p}_{i+1,j}^{n} - \boldsymbol{p}_{i,j}^{n} \right) \qquad [\boldsymbol{4}]$$

$$\boldsymbol{u}_{y_{i+\frac{1}{2},j}}^{n+\frac{1}{2}} = \boldsymbol{u}_{y_{i+\frac{1}{2},j}}^{n-\frac{1}{2}} - \frac{\Delta \boldsymbol{t}}{\boldsymbol{\rho}\Delta} \left(\boldsymbol{p}_{i+1,j}^{n} - \boldsymbol{p}_{i,j}^{n} \right) \qquad [\boldsymbol{5}]$$

where Δ is the grid interval and $\Delta \boldsymbol{t}$ is the time resolution. The terms $\boldsymbol{p}_{i,j}^{n}$, $\boldsymbol{u}_{x_{i,j}}^{n}$, and $\boldsymbol{u}_{y_{i,j}}^{n}$ are the sound pressure and particle velocity at a position (x, y) = (iΔ, jΔ) and time t = n$\Delta \boldsymbol{t}$, respectively. The sound propagation is calculated by alternately solving equations [3], [4], and [5]. In addition, because FDTD is a time- and not a frequency-domain acoustic simulation, diffuse attenuation is included, while the absorption attenuation is not.

Visualization of echo incidence points

Simulation space set-up

In the behavioral experiment, the obstacle walls (acrylic plates) were reaching from the floor to the ceiling, so that bats avoided them by changing their horizontal flight path. To obtain the direction of the bat's pulse emission, a microphone array was placed at a height of 1.2 m. To recreate this setup in our simulation space, we created a two-dimensional space (x–y) on the height level of the array microphones (z = 1.2 m). The FDTD simulation space was located inside the corridor (4.5 m × 1.5 m) as shown in **Supplementary** Fig. S6A, and the absorption boundary condition was the Mur second-order boundary condition [40]. As presented in Table S1, the Courant–Friendrichs–Lewy (CFL) number was 0.57. The spatial resolution (*dx*) was 0.3 mm. And the densities of air and acrylic were 1.29 kg/m^3 and 1.18 kg/m^3, with a bulk modulus of 142.0×10^3 Pa and 8.79×10^9 Pa, respectively.

Echo simulation

To simulate the echoes that returned to the position of the bats' ears, we used information on the bats' pulse emission position and direction obtained from the behavioral experiment. A sinc function signal with a wide frequency band and high time resolution were used in the simulation space as the emitted pulse. It was flat up to 110 kHz and the duration was 0.073 ms (Supplementary Fig. S6B). The sinc function signal was emitted from two source positions (simulating the bat's nostrils), which were set at 1.25 mm each on the left and right side from a given pulse emission position and in the direction of emission which was both obtained from the behavioral experiment (Supplementary Fig. S7A; note that 1.25 mm is based on the half wavelength of the CF2

317 frequency of *R. ferrumequinum nippon* (68 kHz)) [41,42]. Receiver positions (simulating the
318 bat's ears) of the returning echoes in the simulation were set at 10 mm left and right from
319 the pulse emission points (note that 10 mm is based on the distance between the ears of *R.*
320 *ferrumequinum nippon*) (Supplementary Fig. S7A). In the simulation, the impulse
321 responses (echoes) at the two receiver positions were calculated using the FDTD method.
322 Then, the bat's pulse was convolved with these impulse responses to obtain echoes. The
323 bat's pulses in the simulation were the downward FM components created up to the third
324 harmonic, which has been reported to be used for distance discrimination [43]. The
325 downward FM component has a duration of 2 ms and the first harmonic decreases
326 linearly from 34 kHz to 25 kHz, corresponding to the terminal FM component of the
327 echolocation pulse in *R. ferrumequinum nippon* (Supplementary Fig. S7B). The first and
328 third harmonics were set to a sound pressure level of -40 dB based on the second
329 harmonic [44]. The sampling frequency was 2 MHz (1 / dt).
330

331 **Calculation of echo incidence points**

332 Bats estimate the distance to an object based on the time delay between the emitted
333 pulse and the echoes [10,11]. In the simulation, this echo delay was calculated by cross-
334 correlating the simulated left and right echoes with the bat's pulses. The peak value of the
335 autocorrelation of the pulse was normalized, and the peak time above the threshold of the
336 cross-correlating signal was extracted for the left and right echoes (Supplementary Fig.
337 S8). The threshold value was set to 0.02 to detect almost all the peaks. The left and right
338 peak times were matched within a window of the maximum time difference between the

two receiving points (2.5 mm / 340 m/s = 7.4 μs), and combinations of the left and right peak times ([t_r, t_l]) were obtained. The echo incidence points ((x_{echo}, y_{echo})) were then calculated by solving the following two elliptic equations determined by the calculated peak times using the pulse emission positions obtained in the behavioral experiments (i.e., the centers of the two source positions in the simulation) and the left and right receiver positions in the simulation space as the focal points. The pulse emission position was set to $y = 0$ and the direction of pulse emission was set to $x = 0$.

$$\frac{(x_{echo} - x_{r0})^2}{{a_r}^2} + \frac{(y_{echo} - y_{r0})^2}{{b_r}^2} = 1 \quad [6]$$

$$\frac{(x_{echo} - x_{l0})^2}{{a_l}^2} + \frac{(y_{echo} - y_{l0})^2}{{b_l}^2} = 1 \quad [7]$$

$$a_r = \frac{t_r \cdot c_0}{2}, b_r = \sqrt{{a_r}^2 - (x_r - x_{r0})^2}$$

$$a_l = \frac{t_l \cdot c_0}{2}, b_l = \sqrt{{a_l}^2 - (x_l - x_{l0})^2}$$

where x_{r0} is the center position between the pulse emission position and the right receiver position, and x_{l0} is the center position between the pulse emission position and the left receiver position (see Supplementary Fig. S9). An animation of the process of echo incidence point visualization using acoustic simulation is shown in Supplementary Movie S1.

Statistical Analysis

Effect of spatial learning on the echo incidence point distribution

We were interested in testing whether the positions of echo incidence points on the

obstacle walls changed depending on the spatial learning status of the bats (first vs. last flight). Since the bat's task in the behavioral experiment was to avoid the inner sides of the obstacle walls, we considered those echo incidence points that were located on the inner half of the walls and calculated the distance of these points to the inner edge. We modeled this data as a function of the bat's spatial learning status (first vs. last flight) using generalized linear mixed effect models (function glmmTMB, package glmmTMB_1.0.2.1) [45] assuming a negative binomial error distribution (nbinom1) due to overdispersion. Because several echo incidence points can result from one pulse and several pulses were used per bat, we included a random effect with a pulse-ID nested within the bat-ID. The quality of the model fit was graphically examined (function in package DHARMa_0.3.3.0) [46] and its overall significance was determined by comparing it to the respective null model that contains only the random effect via a χ^2-test (function anova in stats) [47]. The significance of the factor coding for the bat's experience was derived from a type-II-Wald- χ^2-test (function anova, package car_3.0-10) [48] while the factor-levels were compared based on least-square-means (function lsmeans, package emmeans_1.5.4) [49]. The statistical significance level was set at $p = 0.05$.

Effects of spatial learning on flight path planning

We calculated the turn rate at 1 ms intervals from the acquired flight paths. The turn rate is the time derivative of the flight path. To investigate the relationship between the turn rate and the pulse and echo direction, respectively, we shifted the turn rate data by a time lag of τ in 10 ms steps from -100 ms (to the left) up to + 600 ms (to the right) relative to the pulse and echo direction, respectively, and calculated the corresponding

correlation coefficients. The 95% confidence intervals for the correlation coefficients were determined by a Fisher transformation of the correlation coefficients to the following ranges

$$\pm z_{\alpha/2} \frac{1}{\sqrt{n-3}} \quad [8]$$

where n represents the number of data and $z_{\alpha/2}$ is 1.96 for 95% confidence interval. Then, we extracted the τ-values that were associated with the highest correlation coefficients for each bat and each category (first vs. last flight) and modeled them on the scale of seconds as a function of the degree of spatial learning (first vs. last flight) in interaction with the factor describing the type of information used by the bat (echo vs. pulse) using linear mixed effect models (function lmer, package lme4_1.1-26) [50]. We added the bat-ID as a random effect to the model due to the repeated sampling of the same individuals. The quality of the model fit, the significance of factors within the model, and the comparisons between factor-levels were conducted using the same functions as mentioned above. The overall model significance was tested against the respective null model using parametric bootstrapping (function PBmodcomp, package pbkrtest_0.5-1.0) [51].

Data Availability

The data used in this study and the code used in the analysis are available at GitHub, https://github.com/tsmyu/Visualization_of_bat_echo_space_by_using_acoustic_simulatio

n.

References

1. Caves, E. M., Brandley, N. C. & Johnsen, S. Visual Acuity and the Evolution of Signals. *Trends Ecol. Evol.* **33**, 358–372 (2018).

2. Taketomi, T., Uchiyama, H. & Ikeda, S. Visual SLAM algorithms: A survey from 2010 to 2016. *IPSJ Transactions on Computer Vision and Applications* vol. 9 (2017).

3. Gordon, A., Li, H., Jonschkowski, R. & Angelova, A. Depth from videos in the wild: Unsupervised monocular depth learning from unknown cameras. in *Proceedings of the IEEE International Conference on Computer Vision* (2019).

4. Griffin, D. R. & Lindsay, R. B. Listening in the Dark. *Phys. Today* **12**, 42–42 (1959).

5. Surlykke, A. & Moss, C. F. Echolocation behavior of big brown bats, Eptesicus fuscus , in the field and the laboratory . *J. Acoust. Soc. Am.* **108**, 2419–2429 (2000).

6. Moss, C. F. & Surlykke, A. Auditory scene analysis by echolocation in bats. *J. Acoust. Soc. Am.* **110**, 2207–2226 (2001).

7. Hiryu, S., Bates, M. E., Simmons, J. A. & Riquimaroux, H. FM echolocating bats shift frequencies to avoid broadcast-echo ambiguity in clutter. *Proc. Natl. Acad. Sci. U. S. A.* **107**, 7048–7053 (2010).

8. Bates, M. E., Simmons, J. A. & Zorikov, T. V. Bats use echo harmonic structure to distinguish their targets from background clutter. *Science (80-.).* **333**, 627–630 (2011).

9. Simmons, J. A. *et al.* Acuity of horizontal angle discrimination by the echolocating bat, Eptesicus fuscus. *J. Comp. Physiol. □ A* **153**, 321–330 (1983).

10. Simmons, J. A. The resolution of target range by echolocating bats. *J. Acoust. Soc. Am.* **54**, 157–173 (1973).

11. Wohlgemuth, M. J., Luo, J. & Moss, C. F. Three-dimensional auditory localization in the echolocating bat. *Curr. Opin. Neurobiol.* **41**, 78–86 (2016).

12. Aytekin, M., Grassi, E., Sahota, M. & Moss, C. F. The bat head-related transfer function reveals binaural cues for sound localization in azimuth and elevation. *J. Acoust. Soc. Am.* **116**, 3594–3605 (2004).

13. Kuc, R. Sensorimotor model of bat echolocation and prey capture. *J. Acoust. Soc. Am.* **96**, 1965–1978 (1994).

14. Vanderelst, D., Holderied, M. W. & Peremans, H. Sensorimotor Model of Obstacle Avoidance in Echolocating Bats. *PLoS Comput. Biol.* **11**, 1–31 (2015).

15. Steckel, J. & Peremans, H. BatSLAM: Simultaneous Localization and Mapping Using Biomimetic Sonar. *PLoS One* **8**, (2013).

16. Yamada, Y. *et al.* Ultrasound navigation based on minimally designed vehicle inspired by the bio-sonar strategy of bats. *Adv. Robot.* **33**, 169–182 (2019).

17. Eliakim, I., Cohen, Z., Kosa, G. & Yovel, Y. A fully autonomous terrestrial bat-like acoustic robot. *PLoS Comput. Biol.* **14**, e1006406 (2018).

18. Mansour, C. B., Koreman, E., Steckel, J., Peremans, H. & Vanderelst, D. Avoidance of non-localizable obstacles in echolocating bats: A robotic model. *PLoS Comput. Biol.* **15**, e1007550 (2019).

19. Greif, S., Zsebok, S., Schmieder, D. & Siemers, B. M. Acoustic mirrors as sensory traps for bats. *Science (80-.).* **357**, 1045–1047 (2017).

20. Simon, R., Holderied, M. W., Koch, C. U. & Von Helversen, O. Floral acoustics: Conspicuous echoes of a dish-shaped leaf attract bat pollinators. *Science (80-.).* **333**, 631–633 (2011).

21. Hiryu, S., Shiori, Y., Hosokawa, T., Riquimaroux, H. & Watanabe, Y. On-board telemetry of emitted sounds from free-flying bats: Compensation for velocity and distance stabilizes echo frequency and amplitude. *J. Comp. Physiol. A Neuroethol. Sensory, Neural, Behav. Physiol.* **194**, 841–851 (2008).

22. Cvikel, N. *et al.* On-board recordings reveal no jamming avoidance in wild bats. *Proc. R. Soc. B Biol. Sci.* **282**, (2015).

23. Yamada, Y. *et al.* Modulation of acoustic navigation behaviour by spatial learning in the echolocating bat Rhinolophus ferrumequinum nippon. *Sci. Rep.* **10**, 1–15 (2020).

24. Ghose, K. & Moss, C. F. Steering by hearing: A bat's acoustic gaze is linked to its flight motor output by a delayed, adaptive linear law. *J. Neurosci.* **26**, 1704–1710 (2006).

25. Land, M. F. Eye movements and the control of actions in everyday life. *Prog. Retin. Eye Res.* **25**, 296–324 (2006).

26. Danilovich, S., Shalev, G., Boonman, A., Goldshtein, A. & Yovel, Y. Echolocating bats detect but misperceive a multidimensional incongruent acoustic stimulus. *Proc. Natl. Acad. Sci.* 202005009 (2020) doi:10.1073/pnas.2005009117.

27. Ulanovsky, N. & Moss, C. F. Hippocampal cellular and network activity in freely moving echolocating bats. *Nat. Neurosci.* **10**, 224–233 (2007).

28. Toledo, S. *et al.* Cognitive map-based navigation in wild bats revealed by a new high-throughput tracking system. *Science (80-.).* **369**, 188–193 (2020).

29. Barchi, J. R., Knowles, J. M. & Simmons, J. A. Spatial memory and stereotypy of flight paths by big brown bats in cluttered surroundings. *J. Exp. Biol.* **216**, 1053–1063 (2013).

30. Yu, C., Luo, J., Wohlgemuth, M. & Moss, C. F. Echolocating bats inspect and discriminate landmark features to guide navigation. *J. Exp. Biol.* **222**, (2019).

31. Gaioni, S. J., Riquimaroux, H. & Suga, N. Biosonar behavior of mustached bats swung on a pendulum prior to cortical ablation. *J. Neurophysiol.* **64**, 1801–1817 (1990).

32. Salles, A., Diebold, C. A. & Moss, C. F. Echolocating bats accumulate information from acoustic snapshots to predict auditory object motion. *Proc. Natl. Acad. Sci.* 202011719 (2020) doi:10.1073/pnas.2011719117.

33. Falk, B., Jakobsen, L., Surlykke, A. & Moss, C. F. Bats coordinate sonar and flight behavior as they forage in open and cluttered environments. *J. Exp. Biol.* **217**, 4356–4364 (2014).

34. D.G.Lowe. Distinctive image features from scale-invariant keypoints. *Int. J. Comput. Vis.* **60**, 91–110 (2004).

35. McMullen, T. A., Simmons, J. A. & Dear, S. P. A computational model of echo processing and acoustic imaging in frequency-modulated echolocating bats: The spectrogram correlationand transformation receiver. *J. Acoust. Soc. Am.* **94**, 2691–2712 (1993).

36. Ming, C., Bates, M. E. & Simmons, J. A. How frequency hopping suppresses pulse-echo ambiguity in bat biosonar. *Proc. Natl. Acad. Sci. U. S. A.* **117**, 17288–17295 (2020).

37. Ming, C., Haro, S., Simmons, A. M. & Simmons, J. A. A comprehensive computational model of animal biosonar signal processing. *PLOS Comput. Biol.* **17**, e1008677 (2021).

38. Yee, K. S. Numerical solution of initial boundary value problems involving Maxwell's equations in isotropic media. *IEEE Trans. Antennas Propag.* **14**, 302–307 (1966).

39. Madariaga, R. Dynamics of an expanding circular fault. *Bull. Seism. Soc. Am.* **66**, 639–666 (1976).

40. Mur, G. Absorbing boundary conditions for the finite-difference approximation of the time-domain electromagnetic-field equations. 377–382 (1981).

508 41. Strother, G. K. & Mogus, M. Acoustical Beam Patterns for Bats: Some Theoretical
509 Considerations. *J. Acoust. Soc. Am.* **48**, 1430–1432 (1970).

510 42. Hartley, D. J. & Suthers, R. A. The sound emission pattern and the acoustical role
511 of the noseleaf in the echolocating bat, Carollia perspicillata. *J. Acoust. Soc. Am.*
512 **82**, 1892–1900 (1987).

513 43. Suga, N. The Extent to Which Biosonar Information Is Represented in the Bat
514 Auditory Cortex. in *Dynamic Aspects of Neocortical Function* 315–373 (John
515 Wiley & Sons, 1984).

516 44. Hartley, D. J. & Suthers, R. A. The acoustics of the vocal tract in the horseshoe bat,
517 Rhinolophus hildebrandti. *J. Acoust. Soc. Am.* **84**, 1201–1213 (1988).

518 45. Brooks, M. E. *et al.* glmmTMB balances speed and flexibility among packages for
519 zero-inflated generalized linear mixed modeling. *R J.* **9**, 378–400 (2017).

520 46. Hartig, F. DHARMa: Residual Diagnostics for Hierarchical (Multi-Level / Mixed)
521 Regression Models. (2020).

522 47. R Core Team. R: A Language and Environment for Statistical Computing. (2021).

523 48. Fox, J. & Weisberg, S. *An {R} Companion to Applied Regression*. (Sage, 2019).

524 49. Lenth, R. V. emmeans: Estimated Marginal Means, aka Least-Squares Means.
525 (2021).

526 50. Bates, D., Mächler, M., Bolker, B. M. & Walker, S. C. Fitting linear mixed-effects
527 models using lme4. *J. Stat. Softw.* **67**, (2015).

528 51. Halekoh, U. & Højsgaard, S. A kenward-Roger approximation and parametric
529 bootstrap methods for tests in linear mixed models-the R package pbkrtest. *J. Stat.*
530 *Softw.* **59**, 1–32 (2014).

531

532 Competing Interest Statement

533 There are no conflicts of interest to declare.

Supplementary Files

This is a list of supplementary files associated with this preprint. Click to download.

- SupplementaryInformation.docx
- MovieS1.mp4